Bull. Chem. Soc. Jpn., 73, 1933—1938 (2000)

Fabrication and Characterization of Meso-Macroporous Anatase TiO_2 Films

Seigo Ito, Shoichiro Yoshida, and Tadashi Watanabe*

Institute of Industrial Science, The University of Tokyo, 7-22-1, Roppongi, Minato-ku, Tokyo 106-8558

(Received March 13, 2000)

A porous TiO_2 film possessing both meso-sized (2—50 nm) pores and macro-sized (100—300 nm) pores has been fabricated for the first time by coating an SnO_2 substrate with a paste consisting of secondary TiO_2 submicroparticles, poyl-ethylene glycol, hydroxypropyl cellulose and water, followed by calcination. The macropores are formed most probably by phase separation between the TiO_2 particles and the polymers in the course of drying of the coated paste. The meso-macroporous TiO_2 film thus prepared has a thickness of ca. 10 μm by four-fold coating, and is characterized by a large surface area arising from the mesopores in the secondary TiO_2 particles, and by the presence of wide channels within the film. The film fabricated by calcination at 550 °C for 30 min was composed of pure anatase with high crystallinity. These features are favorable to construct an electrode for dye-sensitized photoelectrochemical cells.

Recently TiO_2 films have attracted the attention of researchers working on electrodes for solar cells,[1—3] electroluminescence[4] and electrochromic[5] devices, biosensors,[6] and batteries,[7] in view of the high chemical stability, high refractive index, and the high dielectric constant of the oxide.[8] In most cases, the electrode is fabricated from nanocrystalline TiO_2 particles, which ensure a high porosity and activity in comparison with the values for a smooth plane electrode, and the resulting pores are generally of a meso size (2—50 nm), namely between micropores (< 2 nm) and macropores (> 50 nm).[9] One promising area of applications is a photoelectrochemical cell in which dye molecules on the electrode surface inject electrons into TiO_2 upon visible excitation, followed by regeneration of dye molecules by a reducing agent such as I^-, thereby producing a continuous current, as reviewed recently by Kamat,[10] Lampert,[11] and Hagfeldt and Grätzel.[12]

In applications where a redox process plays a key role, the accessibility of a reactant in the solution to the TiO_2 surface is of prime importance.[13,14] The mesopores are normally too narrow for the reactant to access into the depth of the film. Thus, the diffusion coefficient of an electroactive agent in the mesopores is about 10-fold smaller than that in the solvent bulk because of physical hindrances by the wall of the mesopores,[15] and this lowers the efficiency of the output of electrochemical solar cells.[16,17]

Enlargement of mesopores into macropores would promote the diffusion of reactants to a level as in the solvent bulk, and is expected to enhance the output of TiO_2-based dye-sensitized cells. In view of this, Caruso and coworkers have recently fabricated a macroporous TiO_2 film[18—22] with the pore size ranging from 100 nm to 1 μm and a wall thickness of about 100—150 nm.[21,22] However, the surface area of the macroporous film becomes consequently smaller than that of a mesoporous one, and hence deteriorates the photoactivity of the electrode due to the reduced capacity for dye adsorption. To improve the performance of a dye-sensitized solar cell, it is hence desirable to fabricate a TiO_2 film that possesses, at the same time, a large surface area and high accessibility of reactants.

These considerations have incited us to fabricate a novel TiO_2 film (called meso-macroporous film in what follows) possessing both mesopores (2—50 nm in diameter) and macropores (> 50 nm), from anatase TiO_2 secondary submicroparticles. The macropores provide the pathway for reactants, and the mesopores ensure a high surface area of the electrodes. The meso-macroporous films were characterized by scanning electron micrography (SEM), X-ray diffraction (XRD), and specific surface area measurements.

Experimental

Fabrication of TiO_2 Meso-Macroporous Film. Secondary TiO_2 submicroparticles of about 100 nm in diameter were prepared by a hydrothermal treatment described elsewhere.[23] Briefly, a mixture of $Ti[OCH(CH_3)_2]_4$ (10.5 ml, Tokyo Kasei Kogyo), 2-propanol (2 ml, Wako Pure Chemical) and Milli-Q purified H_2O (63 ml) was stirred for 30 min, and then autoclaved at 235 °C for 12 h. Addition of HNO_3 (0.48 ml, Kanto Chemical) was followed by heating at 80 °C for 8 h, and finally drying in a rotary evaporator until the precipitate became powdery.

The submicroparticles were then used to fabricate porous TiO_2 films by a procedure depicted in Fig. 1. A coating paste was prepared from TiO_2 submicroparticles (0.8 g), H_2O (4 ml), polyethylene glycol (PEG, 0.24 g, Junsei Kagaku) and hydroxylpropyl cellulose (HPC, 0.08 g, Tokyo Kasei Kogyo). HPC was used to increase the viscosity of the paste. The SnO_2 substrate 1×4 cm (SnO_2 thickness 900 nm, Nippon Sheet Glass) was fixed on a glass plate (4×7 cm) for heat accumulation and covered along the length of each edge with a piece of adhesive tape (Scotch) having a nominal thickness of 40 μm. A drop of the paste was applied to one of the free edges of the SnO_2 substrate, and flattened with a glass rod sliding

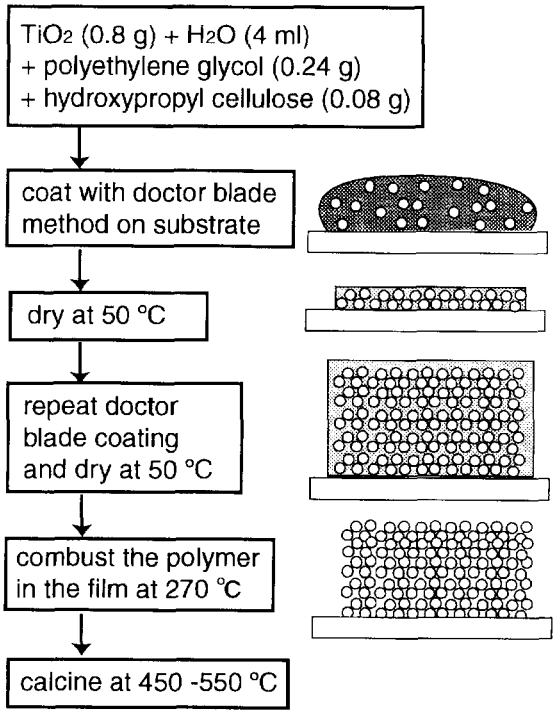

Fig. 1. Flow diagram of meso-macroporous TiO_2 film fabrication.

over the tape-covered edges. Repeated doctor blade coatings[24] of the paste onto an SnO_2 substrate and drying at 50 °C yielded a film. The coatings were repeated while the substrate was hot enough, since coating on a cooled substrate gave a TiO_2 film which easily peeled up and powdered. The glass rod was slid fast for coating the successive overlayers to prevent the underlayer from dissolving into the paste.

The polymers in the film before sintering were combusted at 270 °C for 2 h, and the resulting meso-macroporous TiO_2 film was calcined at 450—550 °C in a tubular ceramic heater, by raising the temperature at a rate of 3 °C min^{-1}. During the heating up, the film became black first, then became semitransparent and lustrous. Though the film usually had visible cracks, it adhered strongly to the substrate. For the purpose of comparison, a mesoporous film was fabricated by use of the TiO_2 sol recommended by the Grätzel group (Ti-Nanoxide T, Solaronix).[24]

Characterization of Secondary TiO_2 Submicroparticles and Meso-Macroporous Film. The secondary TiO_2 submicroparticles and the meso-macroporous films were characterized by XRD (RINT2100, Rigaku), SEM (S-4500, Hitachi), and surface area measurements by nitrogen adsorption (Belsorp 36, Nippon Bell). For XRD measurements, the meso-macroporous films were fabricated under five different heating conditions (at 50 °C for 1 min, at 450, 500, and 550 °C for 30 min, and at 550 °C for 3 h) on silica substrates which do not crystallize from room temperature to 1500 °C, and the XRD patterns were measured from 10 to 80° stepped by 1/4° at room temperature. An SnO_2-coated glass was employed as the film substrate for SEM observation. Observation of the TiO_2 film surface did not require metal sputtering on samples because of the electron reflecting effect due to the TiO_2 conductivity, while the cross section of the TiO_2 film was observed after silver sputtering.

Results

Morphology of the Meso-Macroporous Films. Figure 2 shows the morphology of TiO_2 films before sintering. Since the films have not been combusted, the surface consists of secondary TiO_2 submicroparticles and polymers (HPC and PEG). The TiO_2 network of the slowly dried film (Fig. 2a) is thicker than that of the rapidly dried film (Fig. 2b). The latter film has more macropores (larger than 50 nm in diameter) than the former. As described in Experimental, the slowly dried film (Fig. 2a) became powdery and peeled up by the combustion and sintering. On the other hand, the rapidly dried film with a glass plate for heat accumulation retained the form of a TiO_2 film throughout the combustion and sintering treatments. Therefore, the formation of the TiO_2 film and the stability during the combustion and sintering are dependent on the network morphology of the pre-combusted film.

Figure 3 shows the cross section of a meso-macroporous film prepared by four successive coatings of the paste on an SnO_2 substrate. The TiO_2 film, on top of a 900-nm thick SnO_2 layer (white belt), is darker than the SnO_2 part but brighter than the glass substrate (bottom). This is because the conductivity of the TiO_2 is lower than that of SnO_2. The thickness of the TiO_2 layer is ca. 10.5 μm, which is

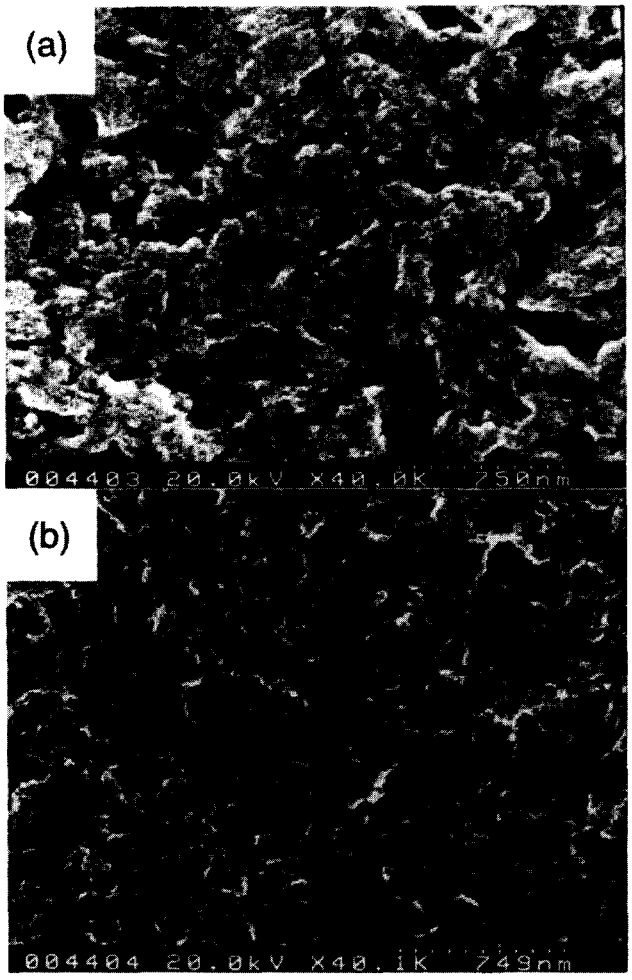

Fig. 2. SEM photograph showing the surface morphology of TiO_2 films before sintering prepared by (a) slow and (b) rapid drying.

Fig. 3. SEM photograph showing the cross section of a TiO_2 film prepared by heating at 450 °C for 30 min on SnO_2-coated glass.

considered to be in an ideal range for use in such applications as photoelectrochemical cells and batteries.

Figure 4 shows the surface morphology of a TiO_2 film prepared by heating at 450 °C for 30 min. It is seen that the film is composed of spherical nanoparticles of about 10 nm in diameter, in agreement with the TEM observation reported previously,[23] which then are aggregated into secondary submicroparticles. The diameter of the secondary submicroparticles in Fig. 4 is about 200 nm, which is larger than that of the starting material (ca. 100 nm as estimated by DLS measurements).[23]

Figure 5 compares the surface morphology of the present meso-macroporous TiO_2 film (Fig. 5a) with a mesoporous TiO_2 film (Fig. 5b). A conspicuous difference is readily noted between the two films. The latter film is fairly smooth and carries mesopores alone, while the former film exhibits large cavities (macropores). The diameter of the macropores in Fig. 5a is about 100—300 nm.

Crystallinity of the Meso-Macroporous Films. Figure 6 depicts the XRD patterns of the meso-macroporous

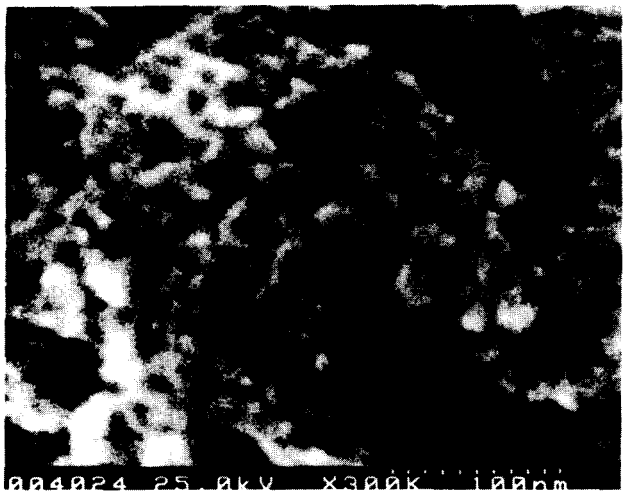

Fig. 4. SEM photograph showing the surface morphology of a TiO_2 film prepared by heating at 450 °C for 30 min.

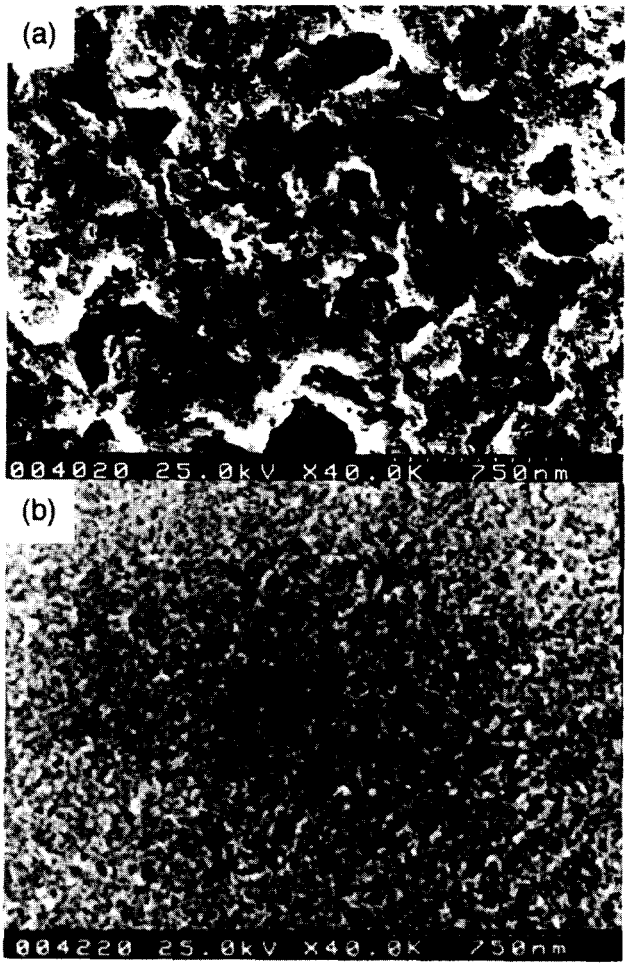

Fig. 5. SEM photographs of (a) a meso-macroporous TiO_2 film prepared by heating at 450 °C for 30 min and (b) a mesoporous TiO_2 film prepared by heating at 450 °C for 30 min.

films. The broad peak at 22° in each trace is attributed to the noncrystalline phase of silica substrates. In the film just after drying at 50 °C, the peaks at 31° and 23° are assignable to the brookite phase[25] and polymers (HPC and PEG), respectively (Fig. 6a).[26,27] All the other easily visible peaks are attributed to anatase.[28] The polymer peak (23°) disappeared by combustion at temperatures above 450 °C (Figs. 6b, c, and d). The small brookite peak (31°) is still visible up to a temperature of 550 °C. By heating at 550 °C for 3 h, the brookite peak disappeared completely, the anatase peaks became sharper, and there appeared a tiny peak at the rutile diffraction position (28°, Fig. 6e).[29]

Change in TiO_2 Surface Area by Sintering Treatments. The surface area of this TiO_2 film was determined by nitrogen adsorption (Table 1). The diameters of the particles are calculated from the surface areas, assuming that the particles are spherical. Hence the surface area (S) and the diameter (d) are correlated by Eq. 1,[30] $S = 6/d\rho$, where ρ (= 3.89 g cm^{-3}) is the density of anatase. The average diameters of the TiO_2 nanoparticles before and after sintering were calculated to be 15.2 and 15.5 nm, respectively. Since the increase in the diameter, arising probably from crystallization and coaptation

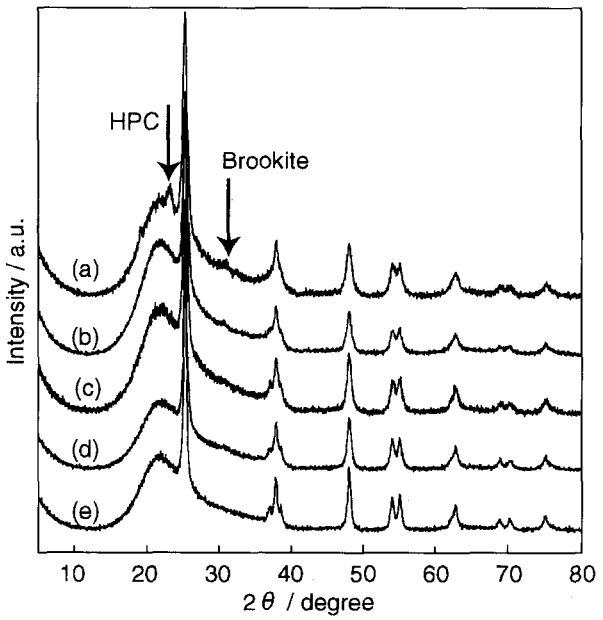

Fig. 6. XRD patterns of TiO_2 films prepared by (a) drying at 50 °C, (b) heating at 450 °C for 30 min, (c) heating at 500 °C for 30 min, (d) heating at 550 °C for 30 min, and (e) heating at 550 °C for 3 h. All the prominent peaks are from anatase.

Table 1. Effect of Sintering Conditions on the Specific Surface Area of the Film and the Diameter of TiO_2 Nanoparticles

Film	Temperature / °C	Time / min	Specific surface area / $m^2\ g^{-1}$	Diameter[a] / nm
Mesoporous	450	30	90.0	17.1
	—	—	101[b]	15.2
Meso-macroporous	450	30	99.6	15.5
	550	30	83.9	18.4
	550	180	46.9	32.9

a) Calculated from specific surface area.[30] b) Powder before sintering.

of the TiO_2 nanoparticles, is small enough, one can conclude that the degree of particle coaptation during sintering is very low and hence there are interspaces (mesopores) preserved between the nanoparticles. When the film was heated at 550 °C for 3 h, the surface area of the meso-macroporous film and the diameter of the TiO_2 nanoparticles were 46.9 $m^2\ g^{-1}$ and 32.9 nm, respectively. The surface area is about half that of the mesoporous film (90.0 $m^2\ g^{-1}$) or the meso-macroporous film (99.6 $m^2\ g^{-1}$) heated at 450 °C for 30 min. This increase in diameter and the decrease in surface area with a rise in temperature indicate the occurrence of shrinkage of TiO_2 nanocrystals resulting from crystallization.[31]

Discussion

Formation of Macropores. The macroporous network was formed during the drying treatment of the TiO_2 paste. Rapid drying yielded numerous macropores and thin networks of TiO_2 submicroparticles (Fig. 2b). On the other hand, slow drying gave a thick network and large dense TiO_2 regions (Fig. 2a). The slow evaporation of water may have allowed TiO_2 particles and the polymer to aggregate, requiring only a small number of holes for passage of water to the exterior, whereas the rapid evaporation may have depressed the aggregation of particles, requiring many holes for passage of water. The dependence of the morphology of the TiO_2 network on the speed of water evaporation could be accounted for in this manner.

In general, peeling up and powdering result from film shrinkage.[32] Shrinkage of the dense TiO_2 region may create large cracks which develop by cohesion of TiO_2 particles; then the film peels up.[32–35] On the other hand, when the TiO_2 network is thin, the cracks are small because of the shrinkage without cohesion of nearby particles. Since the formation of small cracks tends to relieve the cohesive force, the macroscopic shrinkage of the film may be hindered.[33] The pores with a size much larger than the surrounding particles are considered thermodynamically stable and do not shrink during sintering.[36,37] Hence, the fine network (Fig. 2b) stabilizes the film throughout the heating, and the thick network (Fig. 2a) results in peeling up and powdering by combustion and sintering.

Besides the difference in size (monodispersed nanoparticles or secondary submicroparticles), the difference between the mesoporous and meso-macroporous films lies in the addition of hydroxypropyl cellulose (HPC) to increase the viscosity of the coating paste for the latter film. Haga et al.[38] recently suggested that HPC acts in assembling and orienting TiO_2 particles. In view of this, the "walls" of the macroporous regions may have been formed by the secondary TiO_2 particles assembled together by HPC.

Since a dispersion of colloidal particles in water is stabilized by adsorption of polymers on the surface,[39] PEG should exist on the surface of the secondary TiO_2 submicroparticles in the film before sintering (Fig. 2a). The PEG is absent on the surface of TiO_2 particles of the heated films shown in Fig. 4. The combustion of PEG may enlarge the macropores and smooth the trunk of the network. Since the film before sintering contains polymers uniformly, the combustion of the polymers produces the continuity of the macropores in the film from the bottom to the exterior.

The formation mechanism of meso-macroporous films is hence envisaged as follows. Rapid evaporation creates many holes in the film for passage of water from the interior of the film to the exterior. In the course of drying, the secondary TiO_2 particles assemble to HPC and PEG remains on the surface of the TiO_2 network. The succeeding combustion of these polymers yields continuous macropores from the bottom to the exterior of the film and in this step mesopores are reserved in the secondary submicroparticles.

Crystallization of Anatase in Meso-Macroporous Films. Pure anatase nanocrystals are generally considered to be desirable in using TiO_2 films as a semiconductor photoelectrode or photocatalyst, and coexistence of

another crystal phase can provide trapping sites or an energy barrier for electron transfer. The raw material used in the present work (secondary TiO_2 submicroparticles) contained brookite (Fig. 6a),[23] which crystallizes easily by hydrothermal treatments.[40,41] The heat treatment at 450, 500, and 550 °C for 30 min retained the minor brookite phase as seen in Figs. 6b, 6c, and 6d. When the TiO_2 films were heated at 550 °C for 3 h, the brookite phase disappeared completely, to give mono-crystallization of anatase (Fig. 6e). It is known that sintering eliminates brookite and anatase phases, and causes rutile crystallization.[42] The sintered crystallization from brookite to mono-anatase phase is generally difficult, because rutile crystallization occurs before disappearance of brookite.[42] In view of this, mono-crystallization from brookite to anatase, found in the present work, is an unusual phenomenon. This may be because the degree of crystallization of anatase nanoparticles was high enough, and hence they did not change into the rutile phase up to 1000 °C.[43]

Park et al.[44] recently reported that the high crystallinity of rutile annealed at high temperature (500 °C) gave rise to a high dye-sensitization efficiency because of the efficient electron transfer in the TiO_2 network and the diminished energy barriers at the neck portion between the TiO_2 nanoparticles. However, this contradicts a general view that anatase has a higher activity than rutile as a photocatalyst[45] or photoelectrode.[46] Many workers have demonstrated an advantageous feature of porous films of nanocrystalline anatase, obtained by sintering of colloidal anatase nanoparticles at 400 to 450 °C without significant transformation to rutile.[1,2,47—50] However, the anatase nanoparticles used in those works appear to be of low crystallinity. The anatase porous films fabricated in this work, on the other hand, exhibit high crystallinity, due most probably to the high annealing temperature of 550 °C and the prolonged treatment time of 3 h.

As is seen in Table 1, raising the sintering temperature led to a decrease in the surface area and an increase in the average diameter. Similar behavior was also noted by Barbé et al.,[31] who reported that the mesoporous TiO_2 films began to shrink at 350—400 °C, and that the film surface areas were 104 and 88 $m^2 g^{-1}$, by heating at 450 and 550 °C for 30 min, respectively. These values are in good agreement with those of the meso-macroporous films prepared in this work (Table 1). Since these phenomena are due to coaptation of the nanoparticles, the sharpening of XRD anatase patterns with rising temperature (Fig. 6) can be attributed not only to the change of brookite into anatase, but also to the growth and coaptation of the anatase crystals. The diameter (32.9 nm) calculated from the surface area of the film prepared by heating at 550 °C for 3 h is smaller than that of the secondary submicroparticles (ca. 100 nm).[23] This indicates that the nanoparticles are coapted each other, remaining some interspaces (mesopores) between them.

In summary, meso-macroporous TiO_2 films were fabricated from the secondary submicroparticles. It was confirmed that the optimal sintering condition was the heating at 450 °C for 30 min for a large surface TiO_2 film, and at 550 °C for 3 h for a high crystalline anatase TiO_2 film. These meso-macroporous TiO_2 films will be applicable to photoelectrode and photocatalyst because the macropores may facilitate the diffusion of electroactive agents or reactants. An experimental result is to be described elsewhere.[51]

The authors are indebted to Mr. T. Tsuru, Institute of Industrial Science, The University of Tokyo, for specific surface area measurements.

References

1 B. O'Regan and M. Grätzel, *Nature (London)*, **353**, 737 (1991).

2 M. K. Nazzerruddin, A. Kay, I. Podicio, R. Humphy-Baker, E. Müller, P. Liska, N. Vlachopoulos, and M. Grätzel, *J. Am. Chem. Soc.*, **115**, 6382 (1993).

3 U. Bach, D. Lupo, P. Comte, J. E. Moser, F. Weissörtel, J. Salbeck, H. Spreitzer, and M. Grätzel, *Nature (London)*, **395**, 583 (1998).

4 Y. Athanassov, F. P. Rotzinger, P. Péchy, and M. Grätzel, *J. Phys. Chem. B*, **101**, 2552 (1997).

5 F. Pichot, S. Ferrere, R. J. Pitts, and B. A. Gregg, *J. Electrochem. Soc.*, **146**, 4324 (1999).

6 S. Cosnier, A. Senillou, M. Grätzel, P. Comte, N. Vlachopoulos, N. J. Renault, and C. Martelet, *J. Electroanal. Chem.*, **469**, 176 (1999).

7 C. Natarajan, K. Setoguchi, and G. Nogami, *Electrochim. Acta*, **43**, 3371 (1998).

8 "Semiconductor Nanoparticles-Physical, Chemical, and Catalytic Aspects," ed by P. V. Kamat and D. Meisel, Elsevier, Amsterdam (1997).

9 C. A. C. Sequeira and M. J. Hudson, "Multifunctional Mesoporous Inorganic Solids, Mathematical and Physical Sciences," Kluwer, Dordrecht, The Netherlands (1993), Vol. 400, p. 4.

10 P. V. Kamat, *Chem. Rev.*, **93**, 267 (1993).

11 C. M. Lampert, *Sol. Eng. Mater. Sol. Cells*, **32**, 307 (1994).

12 A. Hagfeldt and M. Grätzel, *Chem. Rev.*, **93**, 267 (1993).

13 T. Moritz, J. Reiss, K. Diesner, D. Su, and A. Chemseddine, *J. Phys. Chem. B*, **101**, 8052 (1997).

14 L. Kavan, M. Grätzel, S. E. Gilbert, C. Klemenz, and H. J. Scheel, *J. Am. Chem. Soc.*, **118**, 6716 (1996).

15 Z. Kebede and S.-E. Lindqiust, *Sol. Eng. Mat. Sol. Cells*, **51**, 291 (1998).

16 O. Kohle, M. Grätzel, A. F. Meyer, and T. B. Meyer, *Adv. Mater.*, **9**, 904 (1997).

17 N. Papageorgioiu, Y. Athanassov, M. Armand, P. Bonhôte, H. Pettersson, A. Azam, and M. Grätzel, *J. Electrochem. Soc.*, **143**, 3099 (1996).

18 J. E. G. J. Wijnhoven and W. L. Vos, *Science*, **281**, 802 (1998).

19 B. T. Holland, C. F. Blanford, and A. Stein, *Science*, **281**, 538 (1998).

20 O. D. Velev, T. A. Jede, R. F. Lobo, and A. M. Lenhoff, *Nature (London)*, **389**, 448 (1997).

21 R. A. Caruso, M. Giersig, F. Willig, and M. Antonietti, *Langmuir*, **14**, 6333 (1998).

22 R. A. Caruso, M. Giersig, F. Willig, and M. Antonietti, *Ber. Bunsenges. Phys. Chem.*, **102**, 1540 (1998).

23 S. Ito, S. Yoshida, and T. Watanabe, *Chem. Lett.*, **2000**, 70.

24 S. Y. Huang, G. Schlichthörl, A. J. Nozik, M. Grätzel, and

A. J. Frank, *J. Phys. Chem. B*, **101**, 2576 (1997).

25 "Joint Committee of Powder Diffraction," JCPDS, Card No. 291360.

26 M. Gotić, M. Ivanda, A. Sekulić, S. Musić, S. Popović, A. Turković, and K. Furić, *Mater. Lett.*, **28**, 225 (1996).

27 A. M. Tonejc, M. Goti, B Gržeta, S. Musić, S. Popovi, R. Trojko, A. Turkovi, and I. MuŠević, *Mater. Sci. Eng. B*, **40**, 177 (1996).

28 "Joint Committee of Powder Diffraction," JCPDS, Card No. 211272.

29 "Joint Committee of Powder Diffraction," JCPDS, Card No. 211276.

30 L. Kavan, M. Grätzel, J. Rathouský, and A. Zukal, *J. Electrochem. Soc.*, **143**, 394 (1996).

31 C. J. Barbé, F. Arendse, P. Comte, M. Jirousek, F. Lenzmann, V. Shklover, and M. Gärtzel, *J. Am. Ceram. Soc.*, **80**, 3157 (1997).

32 A. Atkinson and R. M. Guppy, *J. Mater. Sci.*, **26**, 3869 (1991).

33 K. Shinagawa and Y. Hiorashima, *JSNE Inter. J.*, **A42**, 17 (1999).

34 K. Uematsu, M. Miyashita, J.-Y. Kim, and N. Uchida, *J. Am. Ceram. Soc.*, **75**, 1016 (1992).

35 A. G. Evans, *J. Am. Ceram. Soc.*, **65**, 498 (1982).

36 B. J. Kellett and F. F. Lange, *J. Am. Ceram. Soc.*, **71**, 7 (1988).

37 B. J. Kellett and F. F. Lange, *J. Am. Ceram. Soc.*, **72**, 725 (1989).

38 Y. Haga, H. An, and R. Yosomiya, *J. Mater. Sci.*, **32**, 3183 (1997).

39 R. J. Pugh, in "Surface and Colloid Chemistry in Advanced Ceramics Processing," ed by R. J. Pugh and L. Bergström, Marcel Dekker Inc., New York (1994), Chap. 4, pp. 127—192.

40 K. Yanagisawa and J. Ovenstone, *J. Phys. Chem. B*, **103**, 7781 (1999).

41 T. Nagase, T. Ebina, T. Iwasaki, H. Hayashi, Y. Onodera, and M. Chatterjee, *Chem. Lett.*, **1999**, 911.

42 X. Ye, J. Sha, Z. Jiao, and L. Zhang, *Nanostructured Mater.*, **8**, 919 (1997).

43 K. Kato, A. Tsuzuki, H. Taoda, Y. Torii, T. Kato, and Y. Butsugan, *J. Mater. Sci.*, **29**, 5911 (1994).

44 N. G. Park, G. Schlichthorl, J. Van-de-Lagemaat, H. M. Cheong, A. Mascarenhas, and A. J. Frank, *J. Phys. Chem. B*, **103**, 3308 (1999).

45 G. Deo, A. M. Turek, I. E. Wachs, T. Machej, J. Haber, N. Das, H. Eckert, and A. M. Hirt, *Appl. Catal. A*, **91**, 27 (1992).

46 L. Kavan, M. Grätzel, S. E. Gilbert, C. Klemenz, and H. J. Sceel, *J. Am. Chem. Soc.*, **118**, 6716 (1996).

47 A. Hagfeld, N. Vlachopoulos, and M. Gärtzel, *J. Electrochem. Soc.*, **141**, L82 (1994).

48 L. Kavan, K. Kratochvilová, and M. Gärtzel, *J. Electroanal. Chem.*, **394**, 93 (1995).

49 L. Kavan, B. O'Regan, A. Kay, and M. Gärtzel, *J. Electroanal. Chem.*, **346**, 291 (1993).

50 B. O'Regan, J. Moser, M. Anderson, and M. Gärtzel, *J. Phys. Chem.*, **94**, 8720 (1990).

51 S. Ito, K. Ishikawa, C.-J. Wen, S. Yoshida, and T. Watanabe, *Bull. Chem. Soc. Jpn.*, submitted.